THE APPLICATION OF DEEP LEARNING IN LOW-CARBON URBAN LANDSCAPE VEGETATION CONFIGURATION

QIU, W.* – HUANG, Y. Z. – WEI, J. M.

Fujian Forestry Vocational & Technical College, Nanping 353000, Fujian, China
(phone: +86-0599-8461-076; fax: +86-0599-8461-667)

**Corresponding author*
e-mail: ykmjfdkao3@hotmail.com

(Received 24th Jul 2025; accepted 26th Sep 2025)

Abstract. This study proposes EcoDeep-Green, an end-to-end deep learning framework for optimizing low-carbon urban vegetation configuration. By integrating multi-source heterogeneous data, remote sensing, meteorology, soil, urban morphology, and plant traits, the model constructs a high-resolution urban ecological dataset. A CNN-GNN hybrid architecture enables joint spatial-topological feature extraction, while a deep reinforcement learning module formalizes vegetation configuration as a Markov Decision Process to achieve global optimization. Experimental results demonstrate the framework's effectiveness in enhancing carbon sequestration, biodiversity, and planning efficiency, providing a scalable and intelligent solution for sustainable urban ecological design in dynamic environments.
Keywords: *low-carbon, CNN, GNN, deep reinforcement learning, Markov decision process*

Introduction

The accelerating pace of global urbanization is reshaping the structure and function of urban ecosystems. By 2050, approximately 68% of the world's population will reside in urban areas (Hoornweg et al., 2017). While urban expansion drives economic development and societal progress, it simultaneously exacerbates a range of ecological and environmental issues, including elevated greenhouse gas emissions, loss of green spaces, and the intensification of the urban heat island (UHI) effect. Among various mitigation strategies, urban vegetation plays a pivotal role in enhancing carbon sequestration capacity, regulating microclimates, improving biodiversity, and elevating the overall quality of urban life (Edeigba et al., 2024). However, in the context of high-density urban development, the availability of land for vegetation is increasingly constrained. This spatial limitation poses a critical challenge to configure urban vegetation within limited land resources to maximize ecological, climatic, and aesthetic benefits. The optimization of vegetation spatial distribution under multi-constraint, multi-objective conditions has thus emerged as a key problem in contemporary urban ecological planning and sustainable development (Savchenko et al., 2020).

Traditional urban vegetation configuration methods primarily rely on expert knowledge and rule-oriented planning frameworks. Based on landscape design principles, Yılmaz et al. (2018) conducted case studies of several urban parks in Turkey and established a set of vegetation configuration criteria that integrate both functional and aesthetic considerations. However, these methods are heavily dependent on designers' subjective judgment and lack the capacity for quantitatively evaluating the ecological performance of alternative configuration schemes. Şenol et al. (2021) applied GIS-based spatial analysis to assess the accessibility of parks in Izmir, Turkey, identifying suitable vegetation planting zones through multi-scale spatial overlay analysis. They proposed a green space system optimization strategy focused on pedestrian accessibility, but these

http://www.aloki.hu ● ISSN 1589 1623 (Print) ● ISSN 1785 0037 (Online)
DOI: http://dx.doi.org/10.15666/aeer/2306_1116911187

approaches still relied on empirically determined thresholds without incorporating the dynamic processes of vegetation growth. Similarly, Kowe et al. (2021) reviewed the application of remote sensing techniques for monitoring landscape patterns and noted that experience-based vegetation layout strategies frequently overlook the fragmentation of green spaces and its adverse effects on ecosystem functioning. However, their work lacked the development of quantitative analytical tools to address this issue. Johnson et al. (2021) further proposed a conceptual framework of social-ecological system drivers to understand the dynamic evolution of urban forest patches. However, this framework remained largely theoretical and lacked empirical validation.

To overcome the constraints of empirical rule-based methods, researchers have introduced mathematical optimization techniques for urban vegetation configuration. Jia et al. (2023) developed a design and optimization strategy for urban park lighting systems using Internet of Things (IoT) technology. By employing a linear programming model, the method optimized energy consumption and visual performance, indirectly accounting for the influence of vegetation layout on landscape lighting. This demonstrated the feasibility of integrating environmental variables into formal optimization models. Cheng et al. (2025) combined gray statistical analysis with the AHP to construct an evaluation framework for community park landscapes. By quantitatively assessing multiple case studies, the model derived a weighted index system for optimizing landscape elements, offering a structured decision-making framework. However, it remained partially dependent on expert judgment in determining indicator importance, introducing potential bias. Shen et al. (2023) proposed an enhanced ecological corridor identification method by integrating the minimum cumulative resistance model with the gravity model, effectively identifying optimal pathways between ecological nodes. This method emphasized the spatial connectivity of vegetation patches and contributed to urban ecological network planning. However, it does not consider vegetation type and quantity, which may lead to local ecological imbalances.

Recent advances in machine learning (ML) have further expanded the scope of urban vegetation configuration. Ma et al. (2025) utilized random forest models to analyze environmental and vegetation data from ten urban parks in Nanjing, establishing empirical relationships between vegetation growth and environmental factors. However, this model was limited to predictive analysis and did not support spatial configuration optimization. Jahani et al. (2022) applied artificial neural networks to evaluate the aesthetic value of urban park landscapes, modeling visual features, spatial structures, and vegetation compositions. Nevertheless, the model lacked holistic integration of ecological and social variables. Li et al. (2022) proposed a PSO-BP neural network model to automatically assess green space planning schemes, incorporating artificial intelligence into the evaluation process. This method still relied on manually designed scenarios and lacked the capability for automated, intelligent generation of optimized configurations. Wang et al. (2024) applied deep learning to the ecological and architectural analysis of green roofs, constructing predictive models for environmental and structural performance. However, their work focused on a single vegetation type and failed to consider system-wide diversity across urban green infrastructure.

In the domain of visualization and simulation, Chandler et al. (2022) developed immersive landscape modeling technologies to simulate ecological reference scenarios using 3D visualization tools. These tools enhance the intuitive understanding of vegetation effects and support stakeholder decision-making. However, they emphasize representation over optimization and do not incorporate automated algorithms for

http://www.aloki.hu ● ISSN 1589 1623 (Print) ● ISSN 1785 0037 (Online)
DOI: http://dx.doi.org/10.15666/aeer/2306_1116911187

decision support. Niese et al. (2022) proposed a programmatic urban forestry method capable of generating ecologically informed vegetation distribution plans. While this approach merges ecological process modeling with algorithmic design, it lacks adaptive mechanisms for dynamic urban environmental conditions. Xu et al. (2024) employed deep learning techniques to develop a refined blue-green-gray landscape dataset for 36 Chinese cities. Through high-resolution remote sensing analysis, their model accurately identified vegetation, water bodies, and built structures, providing critical data infrastructure for urban ecological research.

Current data-driven approaches to urban landscape optimization face three key challenges. First, most existing methods primarily rely on single-modal data. However, urban environments are inherently multi-dimensional, encompassing landscape imagery, urban layouts, and meteorological information. Reliance on a single modality renders it difficult to achieve optimal configurations. Second, existing methods cannot simultaneously process raster-based spatial data and graph-structured relational data, leading to incomplete representations of spatial dependencies and ecological network structures. Finally, current deep learning–based methods often lack long-term decision-making capabilities and are prone to local optima.

To address these challenges, this study proposes EcoDeep-Green, an end-to-end urban vegetation configuration decision-making framework. Specifically, we first construct a multidimensional urban vegetation dataset and ensure cross-modal consistency through multi-source data fusion and preprocessing. Next, a CNN–GNN hybrid feature extraction architecture is designed, leveraging the spatial feature extraction capability of CNNs and the topological relationship learning capability of GNNs to jointly represent the spatial features of raster data and the ecological relationships of graph structures. Furthermore, the vegetation configuration problem is formalized as a Markov decision process, and a specialized deep Q-network that is adapted to the spatial structure of urban grids is developed to enable sequential decision-making and the search for globally optimal solutions under dynamic, multi-constraint environments. Experimental validation demonstrates that EcoDeep-Green outperforms existing methods in terms of carbon sequestration potential, biodiversity indicators, and planning efficiency.

Materials and methods

Dataset

This study focused on the main urban area of Nanjing, China, constructing a multi-source dataset covering 150 km² of urban vegetation. Nanjing is situated in a subtropical monsoon climate zone, with an average annual temperature of 15.4 °C. As shown in *Table 1*, Annual vegetation observations were collected using both Gaofen-2 (GF-2) satellite imagery and drone imagery. GF-2 imagery, covering the entire year of 2023, has a spatial resolution of 1 m and four spectral bands: blue, green, red, and near-infrared. Drone imagery was acquired with a DJI Phantom 4 RTK equipped with an FC6310R camera, featuring a 20-megapixel 1-inch CMOS sensor capable of RGB and near-infrared imaging at a spatial resolution of 0.1 m. Drone flights were conducted at 120 m altitude using a gridded flight path with 80% frontlap and 70% sidelap to ensure full coverage.

Hourly meteorological observations, including temperature, precipitation, relative humidity, solar radiation, and wind speed, were collected from 15 ground stations in and around Nanjing and aggregated into daily, monthly, and seasonal timescales to align with vegetation growth cycles. Soil samples were collected from 178 points distributed on a

http://www.aloki.hu ● ISSN 1589 1623 (Print) ● ISSN 1785 0037 (Online)
DOI: http://dx.doi.org/10.15666/aeer/2306_1116911187

5 km × 5 km grid at depths of 0–20 cm and 20–40 cm. Measured parameters included soil organic matter (SOM), pH, total nitrogen (TN), total phosphorus (TP), cation exchange capacity (CEC), bulk density, and textural composition, following national standard methods.

Table 1. *The variables used in this paper and their sources*

Variable Type	Specific Indicators	Data Source	Spatial
Building Features	Density, Height, Volume	Nanjing Municipal Planning Bureau	10 m
Transportation Network	Road Density, Type	OpenStreetMap	Vector
Land Use	Land Use Type, Intensity	Planning Database + OSM	10 m
Population Distribution	Population Density	Nanjing Municipal Bureau of Statistics	1 km

Building density, height, and volume were derived from the Nanjing Municipal Planning and Natural Resources Bureau. Spatial features, including road network density and land use types, were extracted from OpenStreetMap. Population density was obtained from 1 km × 1 km gridded data from the 2023 Nanjing census. Species information for 127 common urban vegetation species was collected from the Flora of China database and relevant literature. Field surveys were conducted from June to October 2023 at 10 representative green spaces, such as Purple Mountain, Xuanwu Lake, and the Sun Yat-sen Mausoleum. Surveys recorded ecological parameters including plant height, crown width, leaf area index, phenology, and habitat adaptability, with at least 30 individuals per species sampled.

From July to September 2023, structured questionnaires and interviews were conducted in 15 typical green spaces. The survey included basic personal information (age, occupation, years of residence, etc.), frequency and purpose of green space use, aesthetic evaluation of 20 typical vegetation landscapes on a 7-point Likert scale, and ranking of the importance of eight ecological service functions (e.g., carbon sequestration, cooling, purification, and recreation). A total of 1,800 questionnaires were distributed, with 1,587 valid responses. Descriptive statistics, correlation analysis, and principal component analysis were used to extract public preference characteristics.

All spatial data were projected to the CGCS2000 coordinate system, with registration accuracy better than 0.5 pixels. Spatial resampling was performed using a uniform 50 m × 50 m grid, with bilinear interpolation for continuous data and nearest-neighbor interpolation for categorical data. All variables were normalized to [0,1] using Min-Max normalization to ensure feature comparability. The final dataset comprised 87,465 training samples and 124,638 test samples.

Multi-source data fusion and preprocessing

This study integrates multi-source heterogeneous environmental data to construct a high-resolution, multimodal urban vegetation dataset. The collected data mainly includes remote sensing images, meteorological observations, soil characteristics, urban morphology indicators, and plant species attributes. A systematic preprocessing framework is designed to ensure consistency across different data modalities. High-resolution aerial images obtained via unmanned aerial vehicles (UAVs) serve as a primary source for extracting vegetation-related indices, including the normalized difference vegetation index (NDVI), leaf area index (LAI), and land cover type. The NDVI, which characterizes vegetation health and biomass, is computed as *Equation 1*:

http://www.aloki.hu ● ISSN 1589 1623 (Print) ● ISSN 1785 0037 (Online)
DOI: http://dx.doi.org/10.15666/aeer/2306_1116911187

$$\mathrm{NDVI} = \frac{\rho_{\mathrm{NIR}} - \rho_{\mathrm{Red}}}{\rho_{\mathrm{NIR}} + \rho_{\mathrm{Red}}} \quad \text{(Eq.1)}$$

where ρ_{NIR} and ρ_{Red} represent the reflectance values in the near-infrared and red spectral bands, respectively. Meteorological variables, such as temperature (T), precipitation (P), relative humidity (RH), solar radiation (L), and wind speed (WS), are obtained from ground-based weather stations at an hourly resolution with a spatial granularity of $1\ \mathrm{km}^2$. A plant climate suitability index (CLI) is constructed as *Equation 2*:

$$CLI = f_T(T) + f_P(P) + f_{RH}(RH) + f_L(L) + f_{WS}(WS) \quad \text{(Eq.2)}$$

where f_T, f_P, f_{RH}, f_L, and f_{WS} represent the normalized response functions for each meteorological variable, accounting for plant-specific climatic adaptability. Soil characteristics are collected from representative sample points distributed in a $500\ \mathrm{m} \times 500\ \mathrm{m}$ grid, including parameters such as soil organic matter (SOM), pH, total nitrogen (TN), total phosphorus (TP), and cation exchange capacity (CEC). A comprehensive soil fertility index (SFI) is defined as *Equation 3*:

$$SFI = w_1 \cdot \frac{SOM - SOM_{\min}}{SOM_{\max} - SOM_{\min}} + w_2 \cdot f_{pH}(pH) + \sum_{i=3}^{5} w_i \cdot \frac{X_i - X_{i,\min}}{X_{i,\max} - X_{i,\min}} \quad \text{(Eq.3)}$$

where $X_i \in TN, TP, CEC$, and $f_{pH}(pH)$ is a nonlinear response function:

$$f_{pH}(pH) = 1 - \frac{|\ pH - pH_{\mathrm{opt}}\ |}{pH_{\mathrm{range}}} \quad \text{(Eq.4)}$$

where pH_{opt} denotes the optimal soil pH for vegetation growth, and pH_{range} defines its acceptable variation range. Urban morphological features are derived from urban planning databases and OpenStreetMap (OSM) data, encompassing building density (BD), road network density (RD), population density (PD), and land use types. The urban heat island intensity (UHI) is modeled as *Equation 5*:

$$UHI = \lambda_1 BD + \lambda_2 RD + \lambda_3 IS + \lambda_4 PD - \lambda_5 GC \quad \text{(Eq.5)}$$

where GC denotes the green space coverage rate, and λ_1 to λ_5 are regression coefficients determined through multiple regression analysis. Plant species attributes, including growth traits, morphological parameters, and ecological adaptability, are integrated from the Flora of China database, literature sources, and field surveys, covering $n = 576$ commonly used urban vegetation species. The carbon sequestration potential (CP_i) of plant species i is estimated as:

$$CP_i = GPP_i \times (1 - R_i) \times S_i \times D_i \quad \text{(Eq.6)}$$

http://www.aloki.hu ● ISSN 1589 1623 (Print) ● ISSN 1785 0037 (Online)
DOI: http://dx.doi.org/10.15666/aeer/2306_1116911187

where GPP_i represents the gross primary productivity, R_i denotes the respiratory loss fraction, S_i is a survival rate adjustment factor, and D_i is a coefficient representing the plant's growth stage. To address the heterogeneity of spatial resolutions, a unified $100\ \mathrm{m} \times 100\ \mathrm{m}$ grid is adopted. Continuous spatial data undergo bilinear interpolation, whereas categorical data utilize nearest-neighbor interpolation. All spatial data are georeferenced to the CGCS2000 coordinate system with a registration accuracy better than 0.5 pixels. The grid cell value $g_{i,j}$ is computed as *Equation 7*:

$$g_{i,j} = \sum_{m,n} w_{m,n} \cdot x_{m,n} \tag{Eq.7}$$

where $w_{m,n}$ denotes the weight coefficient, and $x_{m,n}$ represents the original data value. Meteorological variables are aggregated to obtain daily, monthly, and seasonal statistics. Time-series inconsistencies are corrected using a Kalman filter:

$$\hat{x}t = A_t \hat{x}t - 1 + B_t u_t + K_t (z_t - H_t \hat{x}_{t-1}) \tag{Eq.8}$$

where $\hat{x}_t$ is the state estimate at time t, A_t is the state transition matrix, B_t is the control matrix, u_t is the control vector, K_t is the Kalman gain, z_t is the observed value, and H_t is the observation matrix. Data normalization is performed using Min-Max scaling to ensure comparability across features:

$$x' = \frac{x - \min(X)}{\max(X) - \min(X)} \tag{Eq.9}$$

where X represents a given dataset. The preprocessed multi-source data are structured into a high-order tensor $\mathrm{X} \in \check{} \ ^{I_1 \times I_2 \times \mathrm{L} \times I_N}$, where different data modalities correspond to different tensor dimensions. To enhance feature representation, multi-scale feature extraction is conducted using wavelet transforms:

$$\mathrm{F\,ms} = \sum l = 1^{L} w_l \cdot \mathrm{W}^{-1}(\mathrm{W}_l(\mathrm{X}^{(1)}) \oplus \mathrm{W}_l(\mathrm{X}^{(2)}) \oplus \mathrm{L} \ \oplus \mathrm{W}_l(\mathrm{X}^{(K)})) \tag{Eq.10}$$

where W_l represents the wavelet transform at scale l, W^{-1} denotes the inverse transform, $\oplus$ signifies feature fusion, and w_l is the scale-dependent weight.

CNN-GNN hybrid feature extraction

Urban vegetation configuration optimization involves the integration of raster-based spatial data and relational network data, necessitating a feature extraction framework that can effectively capture both spatial dependencies and topological structures. To address this challenge, this study proposes an innovative CNN-GNN hybrid feature extraction architecture (e.g. *Figure 1*), which fully exploits the intrinsic characteristics of multimodal urban environment and vegetation data. The architecture consists of three core modules: Convolutional Neural Network (CNN) Module responsible for extracting spatial features from rasterized urban environmental data. Graph Neural Network (GNN) Module captures the complex relational dependencies between urban morphology and

http://www.aloki.hu ● ISSN 1589 1623 (Print) ● ISSN 1785 0037 (Online)
DOI: http://dx.doi.org/10.15666/aeer/2306_1116911187

vegetation distribution. Cross-Modal Feature Fusion Module integrates multimodal representations to enhance learning efficacy and joint optimization.

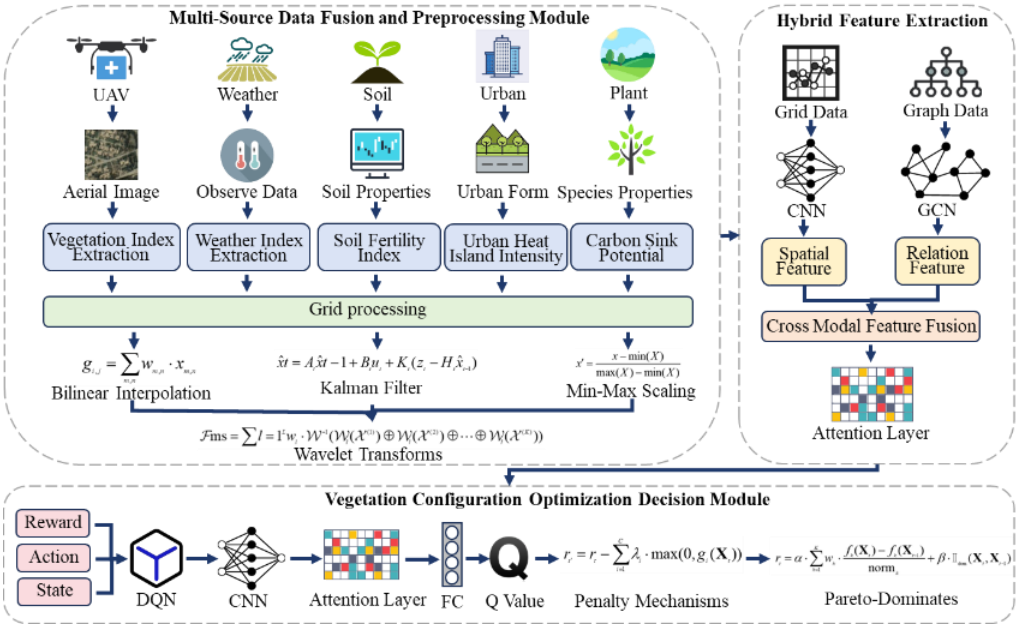

Figure 1. *The end-to-end decision-making framework for urban vegetation configuration*

The overall processing flow follows a "parallel extraction-feature fusion-joint optimization" paradigm, formally expressed as *Equation 11*:

$$\mathbf{F} = \Phi_{\text{fusion}}\left(\Phi_{\text{CNN}}(\mathbf{X}_{\text{grid}}), \Phi_{\text{GNN}}(\mathbf{X}_{\text{graph}})\right) \quad \text{(Eq.11)}$$

where $\mathbf{X}_{\text{grid}}$ and $\mathbf{X}_{\text{graph}}$ represent grid-based and graph-structured data inputs, respectively. The functions Φ_{CNN} and Φ_{GNN} denote the feature extraction processes of CNN and GNN, while Φ_{fusion} represents the cross-modal fusion mechanism, producing the final hybrid feature representation $\mathbf{F}$. To effectively process remote sensing images, meteorological data, and soil attributes, an enhanced residual CNN module is designed based on the ResNet-50 architecture, with modifications tailored for urban vegetation datasets. The backbone network comprises five stages, each containing multiple residual blocks. The forward propagation of residual learning is expressed as *Equation 12*:

$$\mathbf{H}l = \mathrm{F}\ (\mathbf{H}_{l} - 1, \mathbf{W}_{l}) + \mathrm{P}\ (\mathbf{H}_{l} - 1) \quad \text{(Eq.12)}$$

where $\mathbf{H}_{l}$ is the feature map at layer l, $\mathrm{F}(\cdot, \mathbf{W}_{l})$ represents the residual mapping parameterized by the weight matrix $\mathbf{W}_{l}$, and $\mathrm{P}(\cdot)$ denotes the identity mapping (skip connection). To extract multi-scale features, dilated convolution is incorporated, formulated as *Equation 13*:

$$(\mathbf{F} \acute{\mathrm{I}}_{d} \mathbf{k})(p) = \sum_{s+dt=p} \mathbf{F}(s) \cdot \mathbf{k}(t) \quad \text{(Eq.13)}$$

http://www.aloki.hu ● ISSN 1589 1623 (Print) ● ISSN 1785 0037 (Online)
DOI: http://dx.doi.org/10.15666/aeer/2306_1116911187

where $\mathbf{F}$ is the input feature map, $\mathbf{k}$ is the convolution kernel, d is the dilation rate, and p is the output position. The dilation rate sequence $d \in 1,2,4,8$ ensures multi-scale receptive fields, allowing better spatial information extraction. To model the interactions between urban morphology and vegetation, a hierarchical graph learning framework based on Graph Attention Networks (GAT) is developed. The study defines an urban spatial graph as $G=(V,E)$, where V represents grid cells as graph nodes, each characterized by a position vector $\mathbf{p}_i$, environmental attributes $\mathbf{e}_i$, and vegetation features $\mathbf{v}_i$. E denotes edges, constructed based on two relational criteria, Spatial adjacency directly linking adjacent grid cells. Ecological functional similarity establishing long-range connections if vegetation characteristics are sufficiently similar, computed as:

$$\mathrm{sim}(v_i, v_j) = \exp\left(-\frac{|\mathbf{v}_i - \mathbf{v}_j|^2}{2\sigma^2}\right) \quad \text{(Eq.14)}$$

where a threshold τ determines edge existence. The improved GAT mechanism incorporates relational attributes into attention computation:

$$\alpha_{ij} = \frac{\exp\left(\mathrm{LeakyReLU}\left(\mathbf{a}^T[\mathbf{W}\mathbf{h}_i \,|\, \mathbf{W}\mathbf{h}_j \,|\, \mathbf{r}_{ij}]\right)\right)}{\sum k \in \mathrm{N}_i \exp\left(\mathrm{LeakyReLU}\left(\mathbf{a}^T[\mathbf{W}\mathbf{h}_i \,|\, \mathbf{W}\mathbf{h}_k \,|\, \mathbf{r}_{ik}]\right)\right)} \quad \text{(Eq.15)}$$

where $\mathbf{h}_i$ represents the feature of node i, $\mathbf{W}$ is the weight matrix, $\mathbf{a}$ is the attention vector, $\mathbf{r}_{ij}$ is the relational feature, and N_i is the neighbor set. The updated node representation is:

$$\mathbf{h}i' = \sigma\left(\sum j \in \mathrm{N}_i \alpha_{ij} \mathbf{W}\mathbf{h}_j\right) \quad \text{(Eq.16)}$$

where σ denotes the activation function (e.g., ELU). To integrate CNN-extracted spatial features ($\mathbf{F}_{\mathrm{CNN}}$) with GNN-derived relational representations ($\mathbf{F}_{\mathrm{GNN}}$), a cross-attention fusion mechanism is designed. GNN features are mapped back to the spatial grid using:

$$\mathbf{F}_{\mathrm{GNN}}^{\mathrm{grid}} = \mathrm{M}(\mathbf{F}_{\mathrm{GNN}}) \in \check{} \,^{D\times H\times W} \quad \text{(Eq.17)}$$

where M is a spatial mapping function. To align dimensions, 1×1 convolutions are applied:

$$\mathbf{F}_{\mathrm{CNN}}^{\mathrm{adj}} = \mathbf{W}_{\mathrm{CNN}} * \mathbf{F}_{\mathrm{CNN}}, \quad \mathbf{F}_{\mathrm{GNN}}^{\mathrm{adj}} = \mathbf{W}_{\mathrm{GNN}} * \mathbf{F}_{\mathrm{GNN}}^{\mathrm{grid}} \quad \text{(Eq.18)}$$

where $\mathbf{W}_{\mathrm{CNN}}$ and $\mathbf{W}_{\mathrm{GNN}}$ are learnable convolution kernels, and $*$ denotes the convolution operation. The cross-modal attention mechanism computes attention weights between the two feature spaces:

$$\mathbf{A} = \mathrm{softmax}\left(\frac{\mathbf{Q}\mathbf{K}^T}{\sqrt{D'}}\right) \quad \text{(Eq.19)}$$

http://www.aloki.hu ● ISSN 1589 1623 (Print) ● ISSN 1785 0037 (Online)
DOI: http://dx.doi.org/10.15666/aeer/2306_1116911187

where $\mathbf{Q} = \mathbf{W}Q * \mathbf{F}\mathrm{CNN}^{\mathrm{adj}}$ and $\mathbf{K} = \mathbf{W}K * \mathbf{F}\mathrm{GNN}^{\mathrm{adj}}$ represent query and key projections, respectively. The fused representation is computed as:

$$\mathbf{F}_{\mathrm{fused}} = \mathbf{F}_{\mathrm{CNN}}^{\mathrm{adj}} + \mathbf{A} \cdot (\mathbf{W}_{V} * \mathbf{F}_{\mathrm{GNN}}^{\mathrm{adj}}) \quad \text{(Eq.20)}$$

where $\mathbf{W}_{V}$ is a value projection matrix. The CNN-GNN hybrid architecture is trained end-to-end using a composite loss function that jointly optimizes feature extraction quality and prediction accuracy:

$$\mathrm{L}_{\mathrm{total}} = \mathrm{L}_{\mathrm{task}} + \lambda_1 \mathrm{L}_{\mathrm{consist}} + \lambda_2 \mathrm{L}_{\mathrm{reg}} \quad \text{(Eq.21)}$$

where $\mathrm{L}_{\mathrm{task}}$ represents the primary task-specific loss (e.g., carbon sequestration prediction error), $\mathrm{L}_{\mathrm{consistency}}$ ensures representational coherence between CNN and GNN features:

$$\mathrm{L}_{\mathrm{consistency}} = \frac{1}{N} \sum_{i=1}^{N} \| \mathbf{f}_{\mathrm{CNN}}^{i} - \mathbf{f}_{\mathrm{GNN}}^{i} \|_2^2 \quad \text{(Eq.22)}$$

where $\mathrm{L}_{\mathrm{reg}}$ is a regularization term that prevents overfitting:

$$\mathrm{L}_{\mathrm{reg}} = \| \mathbf{W}_{\mathrm{CNN}} \|_F^2 + \| \mathbf{W}_{\mathrm{GNN}} \|_F^2 + \| \mathbf{W} \|_F^2 + \| \mathbf{a} \|_2^2 \quad \text{(Eq.23)}$$

The hyperparameters λ_1 and λ_2 control the relative importance of consistency and regularization, respectively, and are determined through cross-validation.

Vegetation configuration optimization decision module

The vegetation configuration optimization decision module leverages the high-dimensional feature representations extracted by the CNN-GNN hybrid architecture to generate optimal urban vegetation distribution plans. The vegetation configuration problem is formalized as a Markov Decision Process (MDP), defined by the tuple $\mathrm{M} = (S, A, P, R, \gamma)$, where each state $s_t \in S$ represents the vegetation configuration at decision step t, encoded as a multi-channel tensor $s_t \in \check{} \,^{C \times H \times W}$. The channels incorporate both the current partial vegetation configuration matrix $\mathbf{X}_t$ and the comprehensive environmental context derived from the CNN-GNN feature extraction module. Each action $a_t \in A$ corresponds to the assignment of a specific vegetation type $v_j \in V$ to a particular grid cell c_i, represented as $a_t = (c_i, v_j)$. The system transitions deterministically according to $P(s_{t+1} \mid s_t, a_t) = 1$ for the state s_{t+1} that reflects the updated configuration after implementing action a_t. The reward $r_t = R(s_t, a_t, s_{t+1})$ quantifies the immediate benefit of transitioning from state s_t to state s_{t+1} by executing action a_t. It is calculated as the marginal improvement in the multi-objective function value:

$$r_t = F(\mathbf{X}_t) - F(\mathbf{X}_{t-1}) \quad \text{(Eq.24)}$$

where $F(\mathbf{X}_t)$ is a composite objective function:

http://www.aloki.hu ● ISSN 1589 1623 (Print) ● ISSN 1785 0037 (Online)
DOI: http://dx.doi.org/10.15666/aeer/2306_1116911187

$$F(\mathbf{X}_t) = \sum_{k=1}^{K} w_k \cdot f_k(\mathbf{X}_t) \quad \text{(Eq.25)}$$

Here, $f_k(\mathbf{X}_t)$ represents the k -th objective function (e.g., carbon sequestration, biodiversity index, cost efficiency), and w_k is its corresponding weight. We design a specialized DQN architecture that accommodates the spatial characteristics in urban vegetation configuration. The state representation s_t is processed through a multi-channel input layer that preserves spatial relationships and environmental context. A series of convolutional layers extract hierarchical spatial features:

$$\mathbf{H}_l = \text{ReLU}(\text{BN}(\mathbf{W}_l * \mathbf{H}_{l-1} + \mathbf{b}_l)) \quad \text{(Eq.26)}$$

where $\mathbf{H}_l$ is the feature map, $\mathbf{W}_l$ and $\mathbf{b}_l$ are learnable parameters, BN represents batch normalization, and ReLU is the activation function. A self-attention module emphasizes relevant spatial locations and features based on the current configuration state. Decision Network attended features are processed through fully connected layers to estimate the Q-value for each possible action:

$$\mathbf{Q}(s_t, a; \theta) = \mathbf{W}_Q \text{ReLU}(\mathbf{W}_H \text{flatten}(\mathbf{H}_{att}) + \mathbf{b}_H) + \mathbf{b}_Q \quad \text{(Eq.27)}$$

where $\theta = \mathbf{W}_l, \mathbf{b}_l, \mathbf{W}_H, \mathbf{b}_H, \mathbf{W}_Q, \mathbf{b}_Q$ represents all learnable parameters. Urban vegetation configuration is subject to numerous constraints, including budget limitations, spatial compatibility requirements, biodiversity thresholds, and maintenance considerations. To incorporate these constraints into the DRL framework, we employ a penalty-based approach that modifies the reward function:

$$r_t' = r_t - \sum_{i=1}^{C} \lambda_i \cdot \max(0, g_i(\mathbf{X}_t)) \quad \text{(Eq.28)}$$

where $g_i(\mathbf{X}_t) \leq 0$ represents the i -th constraint, and λ_i is the corresponding penalty coefficient. These coefficients are dynamically adjusted during training using an adaptive scheme:

$$\lambda_i^{(k+1)} = \lambda_i^{(k)} \cdot (1 + \delta \cdot \text{sign}(g_i(\mathbf{X}_t))) \quad \text{(Eq.29)}$$

where δ is a small positive constant, and k denotes the iteration number. This approach progressively increases penalty weights for violated constraints while maintaining emphasis on feasible regions of the solution space. For multi-objective optimization, we implement a composite reward function that combines weighted scalar objectives with Pareto dominance considerations:

$$r_t = \alpha \cdot \sum_{k=1}^{K} w_k \cdot \frac{f_k(\mathbf{X}_t) - f_k(\mathbf{X}_{t-1})}{\text{norm}_k} + \beta \cdot \text{I}_{\text{dom}}(\mathbf{X}_t, \mathbf{X}_{t-1}) \quad \text{(Eq.30)}$$

http://www.aloki.hu ● ISSN 1589 1623 (Print) ● ISSN 1785 0037 (Online)
DOI: http://dx.doi.org/10.15666/aeer/2306_1116911187

where $\text{norm}k$ is a normalization factor for objective k, I_{dom} is an indicator function that returns 1 if $\mathbf{X}_t$ Pareto-dominates $\mathbf{X}_{t-1}$ and 0 otherwise, and α and β are weighting parameters.

Experiment and results

Experiment setup

Experimental environment

The core computing server was equipped with an Intel Xeon Platinum 8380 CPU, 1TB of DDR4-3200 ECC RAM, an NVIDIA RTX 4090 GPU, and a hybrid storage system comprising 20TB NVMe SSDs and a 100TB HDD RAID array. For preprocessing and data preparation tasks, a dedicated workstation featuring an AMD Ryzen Threadripper 3990X CPU, 512GB DDR4-3600 memory, an NVIDIA RTX 4090 GPU, and 58TB of SSD storage was utilized. The software environment was built on Ubuntu 22.04 LTS, with distributed computing and deep reinforcement learning handled by Ray 2.5.1.

Model hyperparameter

The CNN module is a modified ResNet-50 with convolution kernel sizes of [7×7, 3×3, 3×3, 3×3, 3×3] and channel configurations of [64, 128, 256, 512, 1024]. It incorporates dilated convolution layers with rates of [1, 2, 4, 8, 16], LeakyReLU activation (slope $\alpha=0.2$), batch normalization (momentum = 0.9), and a CBAM attention mechanism. Max pooling (3×3 kernel, stride 2) is used in the initial layer, and global average pooling concludes the network. Regularization includes a weight decay of 1×10^{-4} and dropout at a rate of 0.3. The GNN module implements a four-layer GAT with node and edge feature dimensions of 128 and 32, respectively. Each layer uses 8 attention heads and hidden layer sizes of [128, 256, 256, 512], combined with ELU activation and residual connections. Graph pooling is conducted via differentiable pooling (DiffPool) at a 0.5 rate, with feature and attention dropout rates of 0.2 and 0.1, respectively. The cross-modal fusion module maps GNN features to the spatial domain using a 1×1 convolution (output channels = 512), applies multi-head cross-attention (8 heads), and merges them into a final 1024-dimensional representation. The deep reinforcement learning module adopts a DQN architecture with hidden layers [1024, 2048, 2048, 1024], ReLU activation, a batch size of 256, and a discount factor $\gamma=0.98$. An ε-greedy exploration strategy is applied, starting with $\varepsilon=1.0$ and decaying linearly to $\varepsilon=0.01$ over 1 million steps. The Adam optimizer is used with an initial learning rate of 3×10^{-4}, decaying to 1×10^{-5}. The training strategy includes 50 epochs of pretraining for CNN and GNN modules, 100 epochs of joint CNN-GNN training, and 500 epochs for full end-to-end model training.

Comparison methods

These include (1) a traditional mathematical programming method (MPM) based on optimization heuristics; (2) a random forest regression model (RFR) serving as a classic ensemble baseline; (3) a standalone CNN that captures only spatial features; (4) a standalone GNN focused on relational structure; (5) a generic DRL model applied without spatial or graph-based preprocessing; (6) a hybrid CNN+MP model combining learned spatial features with rule-based optimization; (7) a CNN+DRL model that integrates

http://www.aloki.hu ● ISSN 1589 1623 (Print) ● ISSN 1785 0037 (Online)
DOI: http://dx.doi.org/10.15666/aeer/2306_1116911187

spatial features into reinforcement learning; and (8) a GNN+DRL model that leverages topological features for decision-making.

Metrics

Carbon Sequestration Potential (CSP) characterizes the annual carbon sequestration capacity of a vegetation configuration scheme, with units of $kgCO_2/m^2/year$. It is calculated as *Equation 31*:

$$\mathrm{CSP} = \sum_{i=1}^{n} A_i \times C_i \times S_i \times G_i \quad \text{(Eq.31)}$$

where A_i is the area covered by the i-th vegetation type (m^2), C_i is the carbon sequestration rate per unit area of the i-th vegetation type ($kgCO_2/m^2/year$), S_i is the survival rate adjustment coefficient based on environmental suitability, and G_i is the plant growth stage coefficient. The Biodiversity Index (BI) assesses species diversity within vegetation communities using a modified Shannon-Wiener index:

$$\mathrm{BI} = H' \times E \times C \quad \text{(Eq.32)}$$

where H' is the Shannon diversity index, E is the evenness index, and C is the connectivity index. The Ecosystem Service Value (ESV) of a vegetation configuration is calculated in $CNY/m^2/year$:

$$\mathrm{ESV} = \sum_{j=1}^{m} \sum_{i=1}^{n} A_i \times V_{ij} \times K_{ij} \quad \text{(Eq.33)}$$

where V_{ij} is the unit value of the j-th ecological service provided by the i-th vegetation type ($CNY/m^2/year$), and K_{ij} is the value adjustment factor based on local environmental conditions. The Implementation Cost (IC) includes the total investment in vegetation procurement, land preparation, planting construction, and maintenance for the first three years (CNY/m^2):

$$\mathrm{IC} = \sum_{i=1}^{n} A_i \times (P_i + L_i + I_i + M_i) \quad \text{(Eq.34)}$$

where P_i is the seedling procurement cost, L_i is the land preparation cost, I_i is the planting construction cost, and M_i is the maintenance and management cost. The Cost-Effectiveness Ratio (CER) measures the comprehensive ecological and economic benefits per unit of input. A larger value indicates higher input-output efficiency:

$$\mathrm{CER} = \frac{\mathrm{ESV} + \mathrm{CSP} \times P_{\mathrm{carbon}}}{\mathrm{IC}} \quad \text{(Eq.35)}$$

where P_{carbon} is the carbon price, calculated as 30 CNY/tCO_2 based on the international carbon trading market.

http://www.aloki.hu ● ISSN 1589 1623 (Print) ● ISSN 1785 0037 (Online)
DOI: http://dx.doi.org/10.15666/aeer/2306_1116911187

Results

Table 2 presents the performance of each method across key evaluation metrics, including carbon sequestration potential (CSP), biodiversity index (BI), ecosystem service value (ESV), implementation cost (IC), and cost-effectiveness ratio (CER). The CNN-GNN-DRL method demonstrated superior performance in all primary metrics. Notably, it achieved a carbon sequestration potential of 4.38 $kgCO_2/m^2$/year, which is 35.2% higher than the MPM baseline, 14.7% higher than the CNN model, and 19.3% higher than the GNN model. For biodiversity index and ecosystem service value, the proposed method reached 0.725 and 102.83CNY/m^2/year, respectively— outperforming all alternatives. Although the implementation cost of CNN-GNN-DRL is relatively high (324.58CNY/m^2), its cost-effectiveness ratio (0.317) remained the best among all methods, indicating that the higher upfront investment yields superior ecological returns over the long term.

Table 2. *Performance comparison of different methods on main evaluation indicators*

Method	CSP	BI	ESV	IC	CER	Composite Index
MPM	3.24	0.548	76.42	286.35	68.25	0.63
RFR	3.58	0.612	85.73	295.68	72.47	0.681
CNN	3.82	0.635	92.46	308.42	75.32	0.716
GNN	3.67	0.673	89.37	304.67	76.58	0.723
DRL	3.74	0.651	90.63	312.54	74.89	0.719
CNN+MP	3.95	0.668	94.28	315.36	78.42	0.742
CNN+DRL	4.12	0.682	97.53	318.72	80.65	0.758
GNN+DRL	4.05	0.698	96.42	319.46	81.24	0.764
CNN-GNN-DRL	4.38	0.725	102.83	321.58	84.73	0.796

To further assess multi-objective optimization capabilities, Pareto frontier analysis and hypervolume metrics were employed. The Pareto front describes the set of optimal solutions in multi-objective optimization problems. *Figure 2* illustrates the Pareto boundaries across three core objectives: carbon sink potential, biodiversity index, and implementation cost. The CNN-GNN-DRL method produced a broader and more comprehensive Pareto front, covering a significantly larger solution space in the three-dimensional objective domain. This indicates its strong capacity for identifying well-balanced, globally optimal solutions that effectively navigate trade-offs between ecological performance and economic constraints.

In addition to macro-level evaluation, model performance was assessed at the micro-level through vegetation suitability prediction. Five representative urban vegetation types were selected, and *Table 3* reports the predictive accuracy of each method. The CNN-GNN-DRL framework achieved the highest average accuracy of 90.13%, with exceptional results for herbaceous (93.78%) and shrub communities (92.65%). Even for mixed forest types, which are characterized by high structural and ecological complexity, the method achieved an accuracy of 85.37%—a 20.09% improvement over the traditional MPM method.

To investigate the internal contribution of model components, ablation studies were conducted by systematically removing or replacing key modules. As shown in *Figure 3*, both CNN and GNN modules played critical roles in performance. Removing the GNN module resulted in a performance drop of 0.072 in the composite index, while removal of

http://www.aloki.hu ● ISSN 1589 1623 (Print) ● ISSN 1785 0037 (Online)
DOI: http://dx.doi.org/10.15666/aeer/2306_1116911187

the CNN module caused a 0.065 decline, confirming the necessity of integrating spatial and topological information. Replacing the cross-modal attention mechanism with simple feature concatenation led to a 0.043 drop, underscoring the effectiveness of the attention-based fusion strategy. The inclusion of a multi-objective reward function and dynamic constraint handling contributed an additional 0.038 and 0.035 performance gain, respectively, highlighting the importance of learning-aware decision processes and adaptive trade-off balancing.

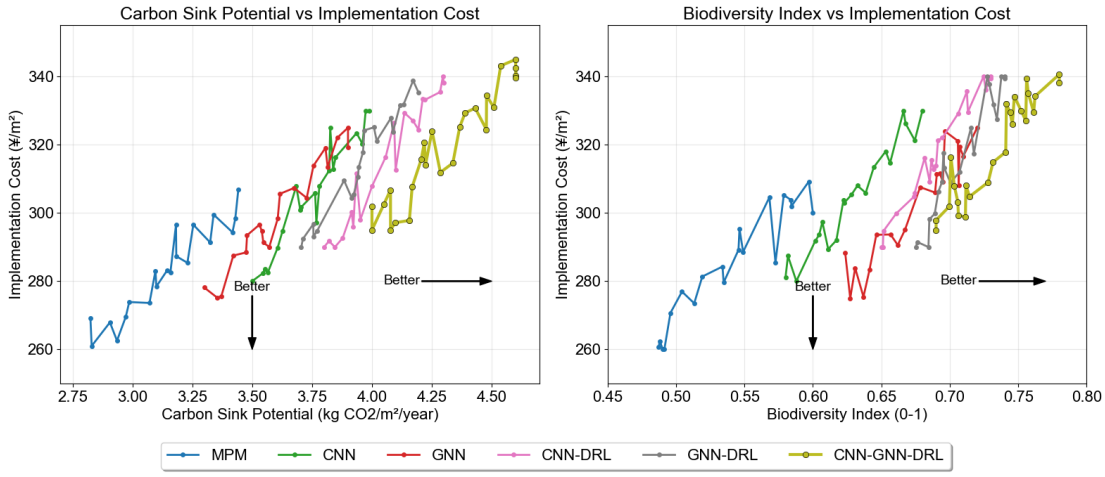

Figure 2. *Pareto frontiers for different optimization methods*

Table 3. *Comparison of the accuracy of different methods in predicting suitability (%)*

Method	Deciduous broad-leaved	Evergreen broad-leaved	Mixed	Shrub	Herb
MPM	72.38	68.57	65.28	74.73	71.41
RFR	78.52	75.26	71.83	80.15	82.47
CNN	83.54	79.48	76.31	84.76	87.18
GNN	81.76	77.85	75.62	83.27	85.62
DRL	80.38	76.42	73.87	82.64	80.82
CNN+MP	84.73	81.37	68.59	88.42	83.91
CNN+DRL	87.26	84.47	81.28	90.35	86.22
GNN+DRL	86.58	82.95	80.64	89.82	85.49
CNN-GNN-DRL	91.03	87.64	85.37	93.72	90.13

Model robustness under environmental perturbation was evaluated to simulate real-world disturbances such as climate variability, urban expansion, and extreme weather events. Controlled perturbations were introduced to test data, and the results are presented in *Figure 4*. As the degree of disturbance increased, all models exhibited performance degradation. However, CNN-GNN-DRL showed the highest resilience, with only an 8.7% performance reduction under 20% disturbance, compared to 28.3% for MPM, 18.5% for CNN, and 17.2% for GNN. This robustness is attributed to the model's capacity to learn high-dimensional, cross-modal feature representations that encode complex environment–vegetation interactions and enable stable decision-making under uncertainty.

http://www.aloki.hu ● ISSN 1589 1623 (Print) ● ISSN 1785 0037 (Online)
DOI: http://dx.doi.org/10.15666/aeer/2306_1116911187

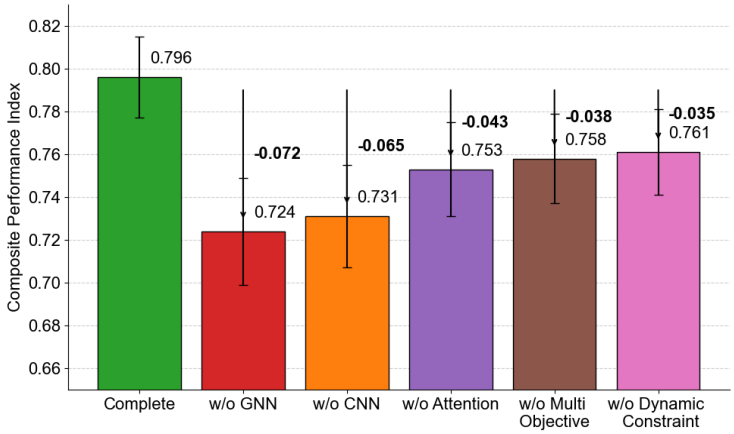

Figure 3. *Ablation study: impact of component removal*

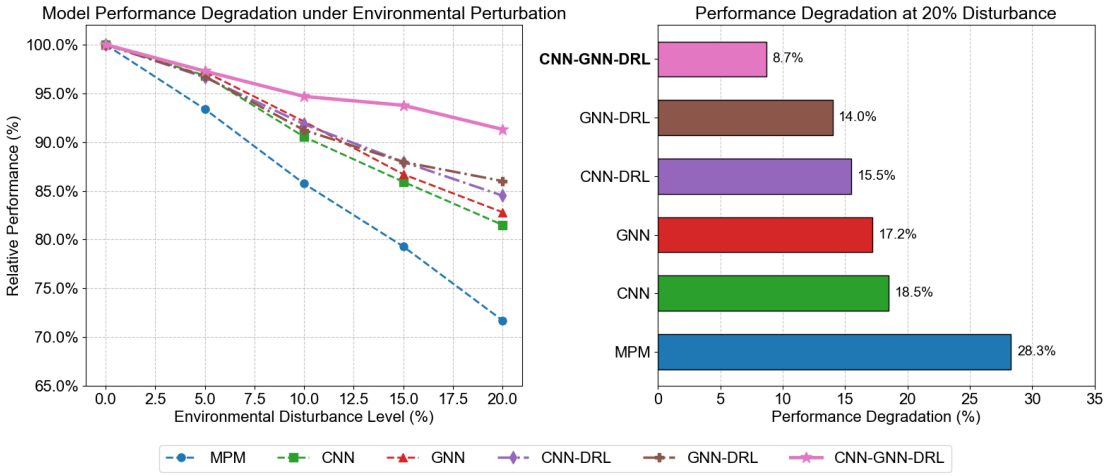

Figure 4. *Model robustness to environmental perturbation*

Scalability and computational efficiency were also evaluated, as they are crucial for city-scale vegetation planning. *Table 4* shows that for small-scale optimization (1 km²), the MPM method was the fastest (0.8 minutes), while CNN-GNN-DRL required 6.4 minutes. However, as the spatial scale increased, CNN-GNN-DRL demonstrated superior scalability. The scalability coefficient (time per unit area) was 3.25 for CNN-GNN-DRL, outperforming all other methods and indicating better relative efficiency in large-scale applications. Although memory usage was relatively high at 18.7GB, this demand is manageable with modern high-performance systems. Moreover, CNN-GNN-DRL supports parallelization, and in an 8-GPU distributed setup, optimization for a 100km² region was completed in approximately 7.5 hours—well within practical urban planning timelines.

To assess the practical application value of the framework, a real-world case study was conducted in the Purple Mountain region of Nanjing (15 km²). The CNN-GNN-DRL method was applied to generate an optimized vegetation configuration plan and compared with the existing layout. As shown in *Figure 5* and *Figure 6*, the optimized scheme resulted in a more coherent spatial structure. Key improvements included: (1) enhanced ecological corridor connectivity, (2) optimized vegetation type distribution based on

http://www.aloki.hu ● ISSN 1589 1623 (Print) ● ISSN 1785 0037 (Online)
DOI: http://dx.doi.org/10.15666/aeer/2306_1116911187

environmental gradients and urban morphology, and (3) the establishment of ecotone buffer zones to mitigate urban expansion impacts. *Figure 6* illustrates statistically significant improvements ($p < 0.001$) across all core ecological indicators, with carbon sink potential, landscape connectivity, and heat island mitigation increased by over 50%, and maintenance complexity reduced by 23.28%. Public satisfaction increased by 15.45%, as reflected in post-optimization surveys. Feedback emphasized improvements in visual diversity, seasonal variation, and spatial comfort in recreational areas.

Table 4. *Comparison of computational efficiency and scalability of different methods*

Method	Small Area	Medium Area	Large Area	Scalability Factor	Memory
MPM	0.81	28.57	18.72	3.65	2.38
RFR	1.29	36.82	22.53	3.72	3.81
CNN	2.54	48.38	27.63	3.48	8.51
GNN	2.85	52.57	29.38	3.42	9.28
DRL	3.26	56.82	31.57	3.48	7.81
CNN+MP	35.91	62.49	34.29	3.38	10.61
CNN+DRL	4.84	78.69	42.73	3.31	14.28
GNN+DRL	5.27	82.18	44.59	3.37	15.19
CNN-GNN-DRL	6.49	94.81	48.27	3.26	18.72

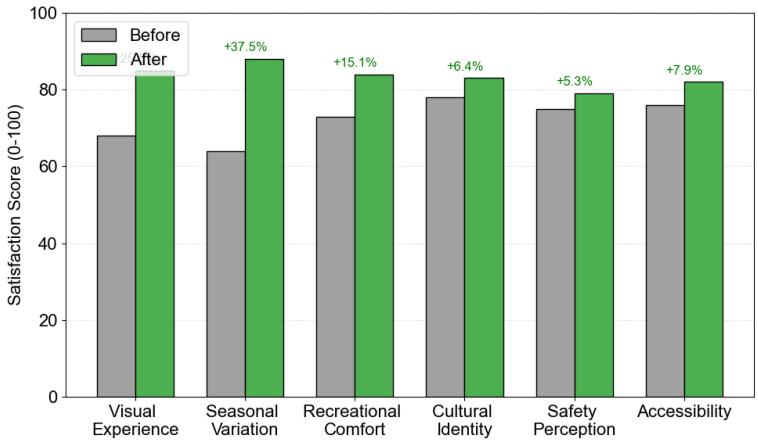

Figure 5. *Public satisfaction components before and after optimization*

To visually compare spatial optimization outcomes, vegetation configuration maps for a representative 2 km×2 km area in central Nanjing were generated, as shown in *Figure 7*. Traditional methods such as MPM and RFR produced relatively rigid and patchy layouts, reflecting limited adaptability to urban morphology and lacking alignment with ecological connectivity principles. While the CNN model showed improved sensitivity to local environmental conditions, it struggled to ensure spatial continuity at larger scales, resulting in fragmented layouts. Conversely, the GNN model performed better in maintaining topological integrity of green space networks but lacked granularity in microclimatic adaptation. The proposed CNN-GNN-DRL method effectively integrated both local environmental heterogeneity and global spatial structures, generating vegetation layouts that adapt to build environment variations while preserving ecological

http://www.aloki.hu ● ISSN 1589 1623 (Print) ● ISSN 1785 0037 (Online)
DOI: http://dx.doi.org/10.15666/aeer/2306_1116911187

coherence. Especially in transition zones between high-density urban blocks and open spaces, the method dynamically allocated vegetation types and densities to form ecological corridors, buffer zones, and functionally graded green systems, thereby enhancing overall ecosystem performance.

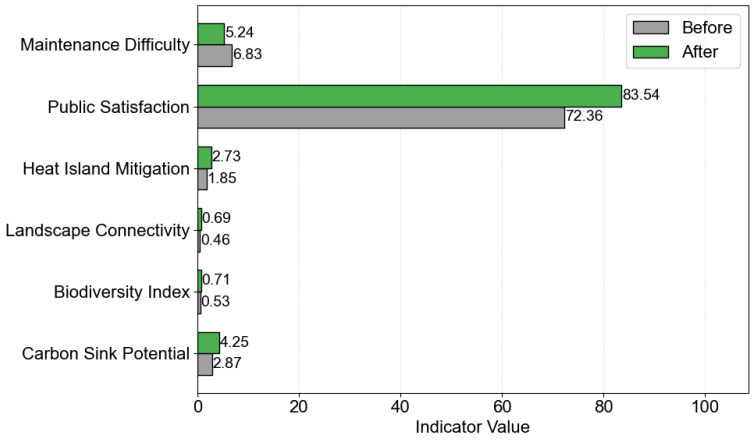

Figure 6. *Ecological and social indicators before and after optimization*

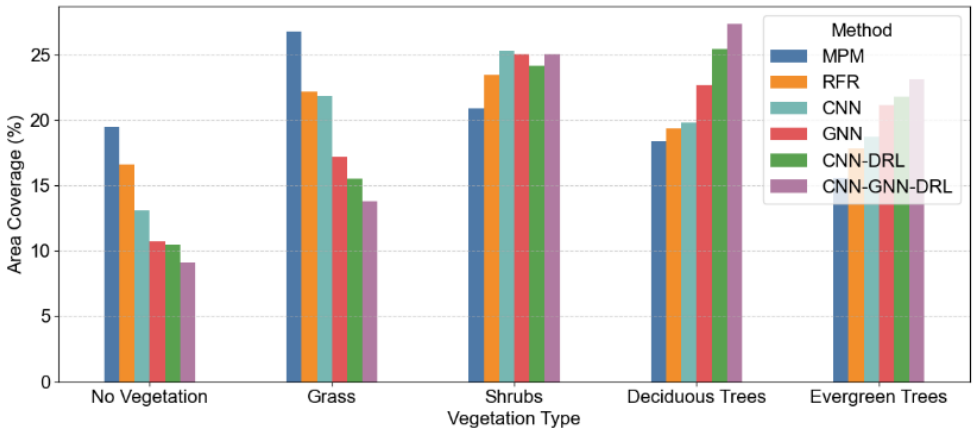

Figure 7. *Comparison of vegetation optimization methods: spatial pattern analysis*

Conclusion

This study presents a novel deep learning–based framework, EcoDeep-Green, for intelligent low-carbon urban vegetation configuration. By integrating multi-source heterogeneous environmental data and designing a hybrid CNN-GNN feature extraction architecture, the framework effectively captures the spatial heterogeneity and ecological dependencies inherent in urban ecosystems. Furthermore, by modeling the configuration task as a Markov Decision Process and applying a deep reinforcement learning strategy, EcoDeep-Green achieves global optimization under dynamic, and multi-objective constraints. Experimental validation demonstrates the framework's performance in enhancing carbon sequestration potential, improving biodiversity, and optimizing urban ecological planning efficiency. However, several limitations remain. First, the current framework primarily focuses on biophysical and environmental variables, while sociocultural and economic factors—such as public preferences, land-use policies, and

http://www.aloki.hu ● ISSN 1589 1623 (Print) ● ISSN 1785 0037 (Online)
DOI: http://dx.doi.org/10.15666/aeer/2306_1116911187

maintenance costs—are not yet fully integrated. Second, the generalizability of the trained model across diverse urban contexts (e.g., climate zones, urban forms) requires further validation. Third, although the proposed DRL-based decision module improves long-term planning capabilities, its interpretability and stability under real-time deployment conditions warrant additional investigation. Future work will focus on three directions: (1) expanding the framework to incorporate socio-economic data and participatory planning inputs, thereby enhancing its comprehensiveness and policy relevance; (2) developing a transfer learning mechanism to support model generalization across cities with limited local data; and (3) integrating real-time data streams (e.g., IoT sensors, weather forecasts) to support dynamic, adaptive vegetation configuration in response to changing environmental conditions.

Acknowledgements. This research supported by Fujian Forestry Vocational & Technical College course ideological and political teaching research project: Ideological and political Teaching innovation of Landscape Design under the perspective of Artificial Intelligence (KCSZJY202403).

REFERENCES

[1] Chandler, T., Richards, A. E., Jenny, B., Dickson, F., Huang, J., Klippel, A., Neylan, M., Wang, F., Prober, S. M. (2022): Immersive landscapes: modelling ecosystem reference conditions in virtual reality. – Landscape Ecology 37: 1293-1309.

[2] Cheng, Q., Li, Q. (2025): The application of grey statistical method and analytic hierarchy process in the evaluation of community park rehabilitation landscapes. – Humanities and Social Sciences Communications 12(1): 1-10.

[3] Edeigba, B. A., Ashinze, U. K., Umoh, A. A., Biu, P. W., Preye, W., Daraojimba, A. I. (2024): Urban green spaces and their impact on environmental health: A Global Review. – World J. Adv. Res. Rev 21: 917-927.

[4] Hoornweg, D., Pope, K. (2017): Population predictions for the world's largest cities in the 21st century. – Environment and Urbanization 29(1): 195-216.

[5] Jahani, A., Allahverdi, S., Saffariha, M., Alitavoli, A., Ghiyasi, S. (2022): Environmental modeling of landscape aesthetic value in natural urban parks using artificial neural network technique. – Modeling Earth Systems and Environment 8(1): 163-172.

[6] Jia, W., Zhang, M. (2023): Design and Optimization of Landscape Lighting in Urban Parks using Internet of Things Technology. – Computer-Aided Design & Applications 20: 58-70.

[7] Johnson, L. R., Johnson, M. L., Aronson, M. F. J., Campbell, L. K., Carr, M. E., Clarke, M., D'Amico, V., Darling, L., Erker, T., Fahey, R. T. (2021): Conceptualizing social-ecological drivers of change in urban forest patches. – Urban Ecosystems 24: 633-648.

[8] Kowe, P., Mutanga, O., Dube, T. (2021): Advancements in the remote sensing of landscape pattern of urban green spaces and vegetation fragmentation. – International Journal of Remote Sensing 42(10): 3797-3832.

[9] Li, S., Fan, Z. (2022): Evaluation of urban green space landscape planning scheme based on PSO-BP neural network model. – Alexandria Engineering Journal 61(9): 7141-7153.

[10] Ma, J., Qu, B. (2025): Estimating the predictability of physical activities in urban parks based on landscape morphology—empirical analysis based on 10 urban parks in Nanjing, China. – Landscape Research 50(1): 39-57.

[11] Niese, T., Pirk, S., Albrecht, M., Benes, B., Deussen, O. (2022): Procedural urban forestry. – ACM Transactions on Graphics (TOG) 41(2): 1-18.

[12] Savchenko, A. B., Borodina, T. L. (2020): Green and digital economy for sustainable development of urban areas. – Regional Research of Russia 10: 583-592.

http://www.aloki.hu ● ISSN 1589 1623 (Print) ● ISSN 1785 0037 (Online)
DOI: http://dx.doi.org/10.15666/aeer/2306_1116911187

[13] Şenol, F., Atay Kaya, İ. (2021): GIS-based mappings of park accessibility at multiple spatial scales: a research framework with the case of Izmir (Turkey). – Local Environment 26(11): 1379-1397.
[14] Shen, J., Wang, Y. (2023): An improved method for the identification and setting of ecological corridors in urbanized areas. – Urban Ecosystems 26(1): 141-160.
[15] Wang, C., Guo, J., Liu, J. (2024): Green roofs and their effect on architectural design and urban ecology using deep learning approaches. – Soft Computing 28(4): 3667-3682.
[16] Xu, Z., Zhao, S. (2024): Fine-grained urban blue-green-gray landscape dataset for 36 Chinese cities based on deep learning network. – Scientific Data 11(1): 266-266.
[17] Yılmaz, S., Özgüner, H., Mumcu, S. (2018): An aesthetic approach to planting design in urban parks and greenspaces. – Landscape Research 43(7): 965-983.

http://www.aloki.hu ● ISSN 1589 1623 (Print) ● ISSN 1785 0037 (Online)
DOI: http://dx.doi.org/10.15666/aeer/2306_1116911187